www.sciencemag.org/cgi/content/full/1182174/DC1

Supporting Online Material for

Modulated High-Energy Gamma-Ray Emission from the Microquasar Cygnus X-3

The Fermi LAT Collaboration*

*To whom correspondence should be addressed. E-mail: stephane.corbel@cea.fr (S.C.); Robin.Corbet@nasa.gov (R.C.); Guillaume.Dubus@obs.ujf-grenoble.fr (G.D.)

Published 26 November 2009 on *Science* Express
DOI: 10.1126/science.1182174

This PDF file includes:

Supporting Online Material: 'Modulated High-Energy γ-ray emission from the Microquasar Cygnus X-3'

(See author list in the main paper)

Observations and data analysis

We present the results of LAT observations of the Cygnus region spanning the time range 2008 August 4 to 2009 September 2. For this period we selected the LAT events with energy $>$ 100 MeV and $<$ 100 GeV and matching the *Diffuse* class, that corresponds to standard low-background event selection. We extracted the LAT events from a 15° radius region centered on the position of Cyg X-3. We kept only events with reconstructed zenith angle $\leq$105° in order to reduce the bright gamma-ray albedo from the Earth. In addition, we excluded the time intervals when the observing direction was more than 47° from the zenith (corresponding to periods when the Earth is substantially in the field of view) and when the *Fermi* satellite was within the South Atlantic Anomaly.

We performed an unbinned maximum likelihood spectral analysis with the *LAT* Science Tools (Abdo et al. 2009a) package v9r15p4, using the P6_V3_DIFFUSE instrument response functions. In the analysis we included all LAT point sources within 5° of Cyg X-3 (extracted from the LAT internal 11-month catalog). In addition, we also kept the LAT point sources from 5° to 22° of Cyg X-3 with significance $\geq$ 7 σ and photon flux brighter than 5 $\times$ 10^{-8} ph cm^{-2} s^{-1} above 100 MeV. This results in a total of 27 sources in the model of the Cygnus region. We modeled the LAT point sources with a single power-law with their parameters fixed to their catalog values, except for two pulsars close to Cyg X-3 (PSR J2021+4026 and PSR J2021+3651) for which a better fit was obtained using an exponentially cut-off power-law model. Furthermore, the model includes the Galactic diffuse emission (resulting from cosmic-ray interactions with interstellar medium and radiation) and an isotropic component to model the extragalactic and detector background. The Galactic diffuse emission (model *gll_iem_v02*) is constructed on six galactocentric rings (to account for the non-uniform cosmic-ray flux) with HI, dust and CO surveys and interstellar radiation field. [1]

Cyg X-3 is located at $\sim$ 30 arcminutes from the bright pulsar PSR J2032+4127. We therefore assigned a phase to each LAT photon according to the best available and updated ephemeris (Camilo et

[1]The diffuse model for *LAT* data analysis is provided at http://fermi.gsfc.nasa.gov/ssc/.

al 2009) of PSR J2032+4127. To optimize the search for emission from Cyg X-3, we selected dates from off-pulse phase intervals of PSR J2032+4127. This procedure eliminates all the emission from PSR J2032+4127 at the cost of only 20 % of the *LAT* exposure. We have checked – using the time intervals outside the active periods – that no residual gamma-ray emission was detected at the position of PSR J2032+4127. A level of gamma-ray flux of the order $\sim 0.5 \times 10^{-6}$ ph cm^{-2} s^{-1}, and consistent with stable emission, is detected at the location of Cyg X-3 outside the active periods (see text).

Exposure weighting of power spectra

For *Fermi* light curves, the exposure of time bins is not necessarily uniform. For example, if the time bin size is a lot shorter than the survey repeat time, then there can be extreme differences in the exposure of the time bins. Scargle (1989) noted that the effect of unequally weighted data points in the calculation of a periodogram could be understood by considering the combination of points that coincide in time. This leads to an analogy between a weighted power spectrum and the weighted mean. However, although the procedure to calculate a weighted periodogram is straightforward, it is important that the correct weights are chosen. For example, if source variability is significant compared to the typical errors on data points, then a procedure based on the semi-weighted mean is more generally applicable (Corbet 2007a, b). For *LAT* light curves, the number of photons in a time bin is typically extremely small. If a weight is chosen based on the number of counts in a bin, then bins with the same exposure could receive different weighting. The number of photons for the same underlying count rate will exhibit variations due to Poisson fluctuations and a weighting based on this would also have noise due to this shot noise. For the *LAT* light curves, we therefore used weighting factors based on the relative exposure of the time bins. We calculated the mean count rate of all bins, and then calculated the number of counts expected in each bin based on its exposure. We then adopt an effective error of each bin which is the square root of the number of *predicted* photons divided by the exposure.

Significance of the orbital period

To characterize and assess the significance of the orbital modulation, we performed a Poisson maximum likelihood analysis of the photons extracted from the 1° radius aperture about Cyg X-3 and binned into 1000-second time bins. We modeled the aperture flux as a Fourier expansion in orbital harmonics, giving

the expected counts in a bin centered on time t_i with exposure ϵ_i as:

$$N(t_i) = \epsilon_i \times \left[F_0 + F_1 \cos\left(\frac{t_i - T_0}{P} + \delta_1 \right) + F_2 \cos\left(2\frac{t_i - T_0}{P} + \delta_2 \right) + \ldots \right],$$

where T_0 and P are the zero of orbital phase and period extrapolated to the *LAT* epoch (Singh et al. 2002).

When considering emission from the first (second) active period (see Fig. S1), we found that a sinusoidal model ($F_i = 0$ for $i \geq 2$) improves the log likelihood over a constant model by 11.8 (11.2). Twice the difference in log likelihood is expected to follow a χ^2 distribution with 4 degrees of freedom in the null hypothesis. We verified this distribution with 10^5 simulated light curves and conclude the chance probability of observing a modulation at least this strong is 2.4×10^{-9}.

The addition of a second and third harmonic do not yield statistically significant increases in the likelihood, and we find that modulation in each period is adequately modeled with a sinusoid. As estimated with this model, the phase of maximum of GeV emission for the first (second) period occurs at $\phi = 0.88 \pm 0.03$ ($\phi = 0.76 \pm 0.03$).

We measured the orbital period using a profile likelihood method in which the likelihood was maximized with respect to the parameters F_0, F_1, and δ_1 for each active period (six parameters total) at a fixed orbital period. The best fit period of $P = 0.199655(46)$ days is in good agreement with the extrapolated period.

Finally, using data from quiescent states, we find that a sinusoidal model improves the log likelihood over a constant model by only 0.9, and we conclude there is no evidence for Cyg X-3 orbital modulation outside of the active periods. We also find no evidence for the orbital period in a scan over profile likelihood. The orbital flux minimum around $\phi = 0.3$ is consistent with the baseline flux of the quiescent state (see Fig. 1).

The X-ray states of Cyg X-3

Cyg X-3 displays five distinct spectral states (e.g. Szostek et al. 2008), with frequent transitions between them. Despite the somewhat peculiar spectral shape and low cut-off energy, there is evidence that two of these states belong to the hard and intermediate states, respectively, as seen in black hole binaries (Hjalmarsdotter et al. 2008). The three remaining states (that are globally called the soft state) differ mainly in the spectral index and strength of the spectrum above 10 keV (Szostek et al. 2008, Hjalmarsdotter et

al. 2009). The fact that the *Fermi* active periods (Fig. S2) are seen at times with very high *RXTE*/ASM flux and very low *Swift*/BAT flux (signifying a very soft X-ray spectrum) points to a connection to the soft state also for the high-energy emission. The giant radio flares are always observed in the soft state, with the ultrasoft state (an instance of the soft state) being a prerequisite for the radio flares (Szostek et al. 2008). The connection between *LAT* activity and the strong radio outbursts is important also in the context of the spectral states of Cyg X-3.

Relating the radio flares and the high-energy gamma-ray active periods of Cyg X-3

The radio observations of Cyg X-3 were conducted at 15 GHz with the Arcminute Microkelvin Imager (AMI, Zwart et al. 2008) and the Owens Valley Radio Observatory (OVRO) 40 m telescope. To quantify the relation between the gamma-ray and radio emission, we calculated (Fig. S3) the discrete cross-correlation function (Edelson & Krolik 1988) normalized only by the sample variance. During some LAT active periods of Cyg X-3, there are several radio measurements in a single day only a few hours apart, while the rest of the light curves are sampled every few days, we thus average the radio measurements of each day. For the gamma-rays we use the *LAT* 2-day likelihood analysis light curve using only statistically independent bins (no oversampling). We find a positive correlation between both frequencies with a lag of the radio light curve to the gamma-rays of 5 ± 7 days (the cross-correlation function has been evaluated with a bin sizes of 2 days).

To assess the significance of the peak in the cross-correlation function we simulated the *LAT* light curve and correlated it with the measured radio light curve. A priori, we do not have any knowledge of the noise properties of the *LAT* source coincident with Cyg X-3. If the background count rate fluctuations dominate or if our extraction region includes multiple variable sources in this crowded Cygnus region, then its variation may be white noise. If we simulate white noise of the same variance as the *LAT* measurements (either Gaussian or Bootstrapped), we find that the peak is significant at more than $3\,\sigma$.

However, as the source is connected to Cyg X-3 we have to consider that X-ray binaries usually show red or band limited noise, as also observed in Cyg X-3 (Axelsson et al. 2009). If we assume this is also the case in the gamma-ray regime, we have to incorporate this into our simulations. We therefore created a red noise time-series (Timmer & Koenig 1995) and normalized its variance to the measured variance corrected for the estimated measurement errors. To this light curve, we added artificial measurement errors which are either assumed to be Gaussian or drawn from the distribution of real *LAT* fluxes during

the periods of quiescence. The highest random peaks in the cross-correlation function seem to arise for red noise with an index between 1 and 2. The corresponding one, two and three sigma confidence levels are shown in Fig. S3 (probability to observe the peak given the null-hypotheses of uncorrelated data). Thus, we conclude that the correlation is significant at the 3 σ level.

We note that the cross-correlation is largely dominated by the large radio and gamma-ray flare at the end of the first active period (see Fig. 2). If one excludes this flare, the cross-correlation peaks at mildly positive lag values. The cross-correlation without the flare is, however, not significant (i.e., less than 3 σ).

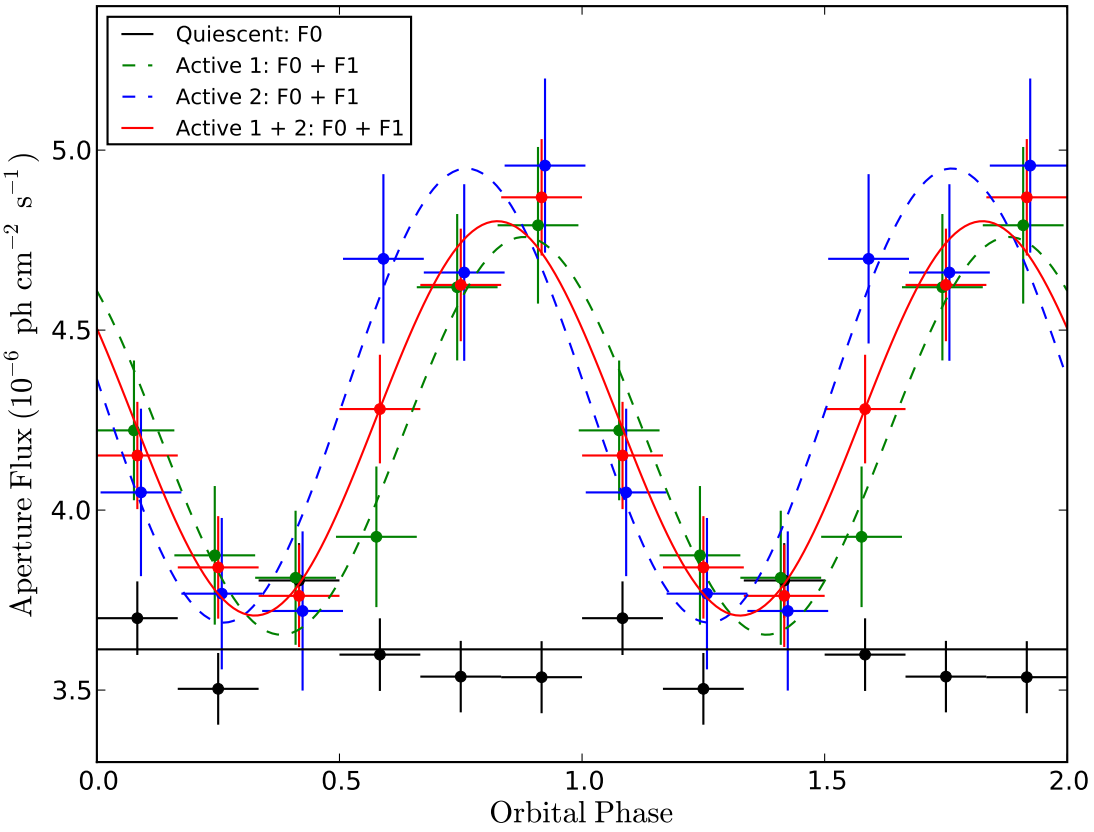

Figure 1: The results of the maximum likelihood fit to the phase-folded data in quiescent (black) and first (green) and second (blue) active periods. The summed emission and a fit to both active periods appears in red. The modulated emission is dominated by a single harmonic, and the minimum flux in the active state is statistically consistent with the emission level (including diffuse emission) within the 1° aperture outside the active periods of Cyg X-3. The flux estimates in six phase bins are shown for reference but were not used in the likelihood fit.

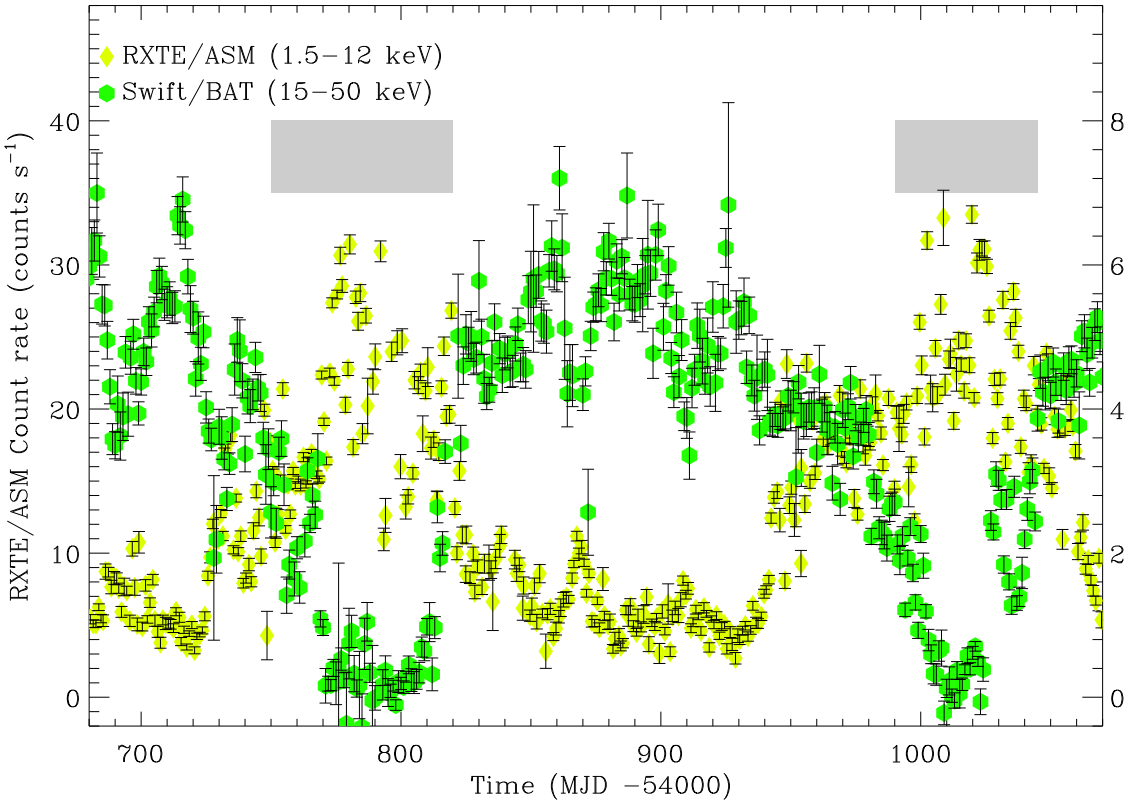

Figure 2: Soft X-ray light curve from *RXTE*/ASM (1.5-12 keV) and hard X-ray light curve from *Swift*/BAT (15-50 keV) corresponding to the period of the *LAT* observations. The right axis corresponds to the scale of the *Swift*/BAT count rate (in 10^{-2} counts s^{-1} cm^{-2}). Two soft X-ray states are observed and they coincide with the period of the *LAT* detection of Cyg X-3 illustrated by the grey bands.

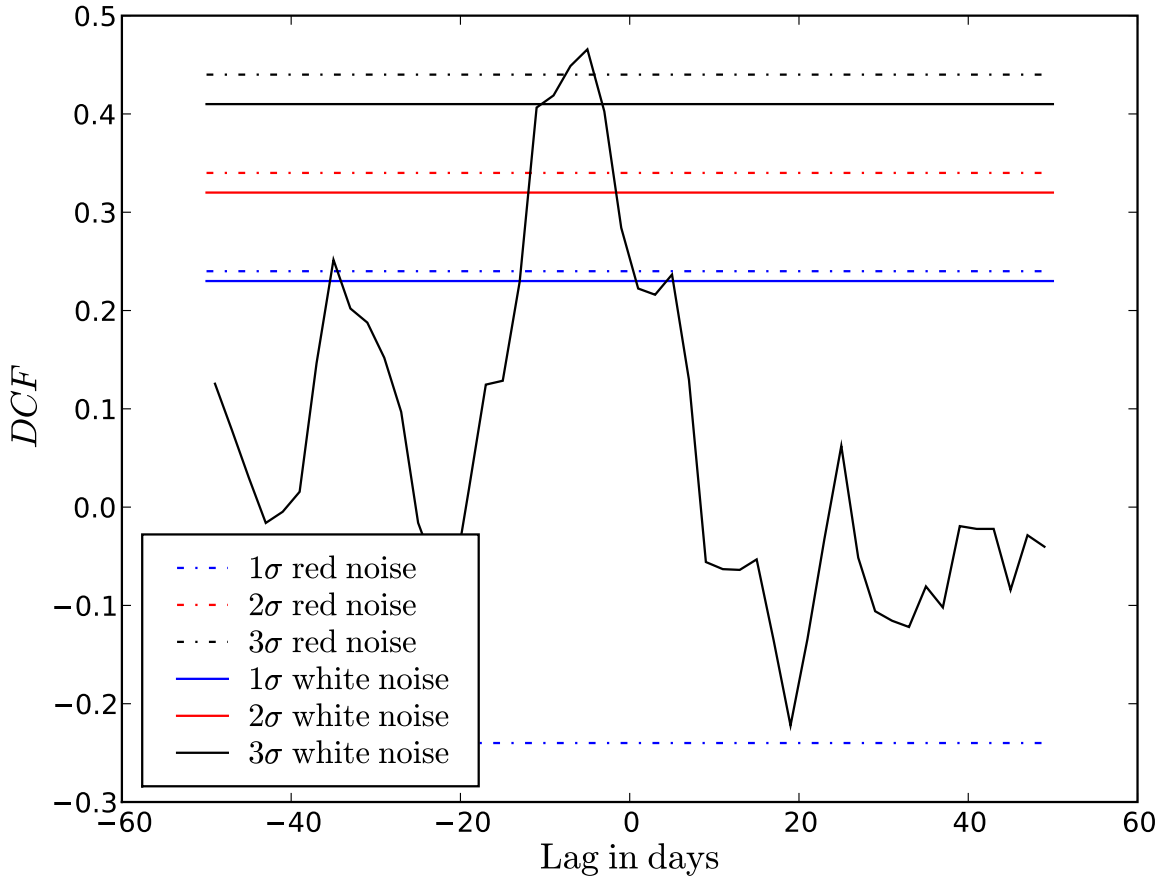

Figure 3: Discrete cross-correlation function (DCF) of the radio and the gamma-ray light curve. The 1 (blue), 2 (red) and 3 (black) σ levels are indicated on the figure assuming white noise (solid lines) or red noise with an index of 1.5 (dashed lines). Negative lags indicate that the radio flux density lags the *LAT* flux.

References and Notes

Axelsson, M., Larsson, A. & Hjalmarsdotter L. *Mon. Not. R. Astron. Soc.*, **394**, 1544 (2009).

Abdo, A. A., et al. *Astrophys. J. Suppl. Ser.*, **183**, 46 (2009a).

Abdo, A. A., et al. *Astrophys. J.*, **701**, L123 (2009b)

Camilo, F., et al., *Astrophys. J.*, **705**, 1 (2009).

Corbet R.H.D. et al. *Astrophys. J.*,, **655**, 458 (2007a).

Corbet R.H.D. et al. *Progress of Theoretical Physics Supplement*, **169**, 200 (2007b)

Edelson, R. A., & Krolik, J. H. *Astrophys. J.*, **333**, 646 (1988).

Hjalmarsdotter L. et al. *Mon. Not. R. Astron. Soc.*, **384**, 278 (2008).

Hjalmarsdotter L. et al., *Mon. Not. R. Astron. Soc.*, **392**, 251(2009).

Levine, A. M., Bradt, H., Cui, W., Jernigan, J. G., Morgan, E. H., Remillard, R., Shirey, R. E., & Smith, D. A. *Astrophys. J.*, **469**, L33 (1996).

Singh, N. S., Naik, S., Paul, B., Agrawal, P. C., Rao, A. R., & Singh, K. Y., *Astron. Astrophys.*, **392**, 161 (2002).

Scargle, J.D. *Astrophys. J.*, **343**, 874 (1989).

Timmer, J., & Koenig, M. *Astron. Astrophys.*, **300**, 707 (1995).

Zwart, J. T. L., et al. , *Mon. Not. R. Astron. Soc.*, **391**, 1545 (2008).